

Alternating Krylov Subspace Image Restoration Methods

J. O. Abad^a, S. Morigi^b, L. Reichel^c, F. Sgallari^{d,*}

^a*Instituto de Ciencia y Tecnologia de Materiales (IMRE), Universidad de La Habana, Habana, Cuba.*

^b*Department of Mathematics, University of Bologna, P.zza Porta S. Donato 5, 40126 Bologna, Italy.*

^c*Department of Mathematical Sciences, Kent State University, Kent, OH 44242, USA.*

^d*Department of Mathematics-CIRAM, University of Bologna, Via Saragozza 8, 40123 Bologna, Italy.*

Abstract

Alternating methods for image deblurring and denoising have recently received considerable attention. The simplest of these methods are two-way methods that restore contaminated images by alternating between deblurring and denoising. This paper describes Krylov subspace-based two-way alternating iterative methods that allow the application of regularization operators different from the identity in both the deblurring and the denoising steps. Numerical examples show that this can improve the quality of the computed restorations. The methods are particularly attractive when matrix-vector products with a discrete blurring operator and its transpose can be evaluated rapidly, but the structure of these operators does not allow inexpensive diagonalization.

Key words: ill-posed problems, deblurring, denoising, alternating iterative method, Krylov method, total variation, edge-preserving regularization

* Corresponding author.

Email addresses: morigi@dm.unibo.it (S. Morigi), reichel@math.kent.edu (L. Reichel), sgallari@dm.unibo.it (F. Sgallari).

1 Introduction

Let the function f^δ represent the available noise- and blur-contaminated image, and let the function \hat{u} represent the associated (unknown) blur- and noise-free image that we would like to recover. We assume the functions f^δ and \hat{u} to be related by the degradation model

$$f^\delta(x) = \int_{\Omega} h(x, y)\hat{u}(y)dy + \eta^\delta(x), \quad x \in \Omega, \quad (1)$$

where Ω is a square or rectangle on which the image is defined, η^δ represents additive noise (error) in the data f^δ , and h is the point-spread function (PSF). The integral may represent a space-invariant or space-variant blurring operator. We would like to recover \hat{u} given the observed image f^δ and the PSF h . The noise η^δ is not known, but we assume that a bound for its norm is available. This helps us to determine the dimension of the Krylov subspace used. However, our solution methods, suitably modified, also can be applied when no bound for the norm of η^δ is known.

We determine an approximation of the desired image \hat{u} by solving a discrete version of a minimization problem of the form

$$\min_{u, w} J(u, w), \quad (2)$$

where

$$J(u, w) := \int_{\Omega} \left(\left(\int_{\Omega} h(x, y)u(y)dy - f^\delta(x) \right)^2 + \alpha (\mathcal{L}(u - w)(x))^2 + \beta |\nabla w(x)| \right) dx, \quad (3)$$

by an alternating iterative method. Minimization in (2) is carried out over suitable linear function spaces. The regularization parameters α and β in (3) are positive constants, and the regularization operator \mathcal{L} may be linear or nonlinear. In the latter case, \mathcal{L} is linearized and updated during the solution process. Two-way alternating iterative methods for the solution of (2) proceed by, for increasing values of the index i , fixing one of the functions, say $w = w^{(i)}$, in (2) and solving for the other function, $u = u^{(i+1)}$, and then solving (2) for $w = w^{(i+1)}$ with $u = u^{(i+1)}$ kept fixed. The iterate $u^{(i+1)}$ is computed by deblurring $w^{(i)}$, and $w^{(i+1)}$ is determined by denoising $u^{(i+1)}$. Starting with $w^{(0)} := f^\delta$, one determines in this manner a sequence of approximate solutions $u^{(1)}, w^{(1)}, u^{(2)}, w^{(2)}, \dots$ of (2).

Alternating iterative image restoration methods have recently received considerable attention; see, e.g., Huang et al. [13], Wen et al. [27], and references

therein. Reasons for their popularity include the ease of design and implementation of these methods, as well as the high quality of the restored images. A main advantage of alternating iterative image restoration schemes is that deblurring and denoising can be carried out independently. Huang et al. [13] describe a two-way alternating iterative method in which regularization is achieved by a TV-norm operator and the identity. This method is generalized by Wen et al. [27] to a three-way alternating scheme that uses TV-norm and wavelet regularization, as well as the identity as regularization operator. Numerical examples in [27] illustrate that using both TV-norm and wavelet regularization, together with the identity regularization operator, can give restorations of higher quality than when using a two-way alternating method that applies either TV-norm or wavelet regularization (but not both) in combination with the identity regularization operator. The methods discussed in [13,27] assume that the discretized blurring operator has a structure that makes fast diagonalization possible, e.g., by the fast Fourier or cosine transforms. A recent application of an alternating iterative method to material identification is described in [14].

This paper presents Krylov subspace-based two-way alternating iterative methods that allow the use of two regularization operators different from the identity. In the computed examples, we use the adaptive total variation method proposed by Chen et al. [7] for denoising. The regularization operator \mathcal{L} is a nonlinear differential operator, which is linearized and updated during the iterations. Computed examples in Section 4 show the nonlinear operator \mathcal{L} to yield more accurate restorations than the identity regularization operator.

Deblurring is carried out by a Krylov subspace iterative method. This method applies a few, say ℓ , steps of Golub-Kahan bidiagonalization to a (large) blurring matrix, H , which is determined by discretization of the integral in (1). Golub-Kahan bidiagonalization yields an orthonormal basis for a Krylov subspace \mathcal{K}_ℓ of dimension ℓ , in which the deblurred image is sought; see Section 2 for details. The discretized and linearized regularization operators obtained from \mathcal{L} are mapped into \mathcal{K}_ℓ . The iterative method so obtained is an extension of the iterative scheme for linear regularization operators described in [12]. The Krylov subspace \mathcal{K}_ℓ is kept fixed in our alternating iterative method. Therefore, the number of matrix-vector product evaluations with the matrix H and its transpose is independent of the number of deblurring steps in our alternating method, and is typically fairly small. This makes the method attractive to apply to problems for which the evaluation of matrix-vector products with H and its transpose is the dominating computational work. We remark that the matrix H is not required to be diagonalizable with the aid of a fast transform. This allows us to restore images with spatially variant blur. The methods described in [13,27] are not well suited for restoration of images with this kind of blur, because they are based on diagonalizing H . The number of bidiagonalization steps, ℓ , is determined with the aid of the discrepancy principle

using the available bound for the error in f^δ . Typically, ℓ is quite small and, in particular, much smaller than the order of H .

Krylov subspace methods that are not based on Golub-Kahan bidiagonalization also can be applied. For instance, when matrix-vector products with the transpose of the matrix H are cumbersome or expensive to evaluate, it may be attractive to replace Golub-Kahan bidiagonalization by the generalized Krylov subspace method described in [24]. Moreover, alternating methods can be implemented within a multilevel framework, e.g., by extending the schemes discussed in [17,18]. However, this is outside the scope of the present paper.

The organization of this paper is as follows. Section 2 describes the alternating methods. Convergence of the methods is shown in Section 3. Our analysis is an adaption of the discussion in Huang et al. [13]. Computed examples are presented in Section 4 and concluding remarks can be found in Section 5.

2 The alternating methods

This section describes our Krylov subspace-based alternating methods and their implementation. Consider a discretization of (1) and let the gray-scale image in the left-hand side of (1) be represented by an array of $n \times n$ pixels. Ordering the pixels column-wise defines a vector in \mathbb{R}^{n^2} , which we also denote by f^δ . The integral operator in (1) is represented by the matrix $H \in \mathbb{R}^{n^2 \times n^2}$, which typically is large. In this discrete setting, our alternating iterative method can be written as

$$u^{(i)} = S_h(w^{(i-1)}) := \operatorname{argmin}_{u \in \mathcal{K}_\ell} \{ \|Hu - f^\delta\|^2 + \alpha \|L^{(i-1)}(u - w^{(i-1)})\|^2 \}, \quad (4)$$

$$w^{(i)} = S_{tv}(u^{(i)}) := \operatorname{argmin}_{w \in \mathbb{R}^{n^2}} \{ \alpha \|L^{(i-1)}(w - u^{(i)})\|^2 + \beta \|w\|_{tv} \}, \quad (5)$$

for $i = 1, 2, 3, \dots$, where $\|\cdot\|_{tv}$ is a vector semi-norm of TV-type. Let the matrix $L^{(i-1)} \in \mathbb{R}^{n^2 \times n^2}$ denote a discretization of the operator \mathcal{L} , and, in case \mathcal{L} is nonlinear, also a linearization. The linearization is updated after each solution of the minimization problem (5); see Subsection 2.2 for details. Our convergence analysis assumes that the matrices $L^{(i-1)}$ are nonsingular. Then both minimization problems (4) and (5) are uniquely solvable. Minimization in (4) is carried out over a suitable ℓ -dimensional Krylov subspace \mathcal{K}_ℓ defined below. Throughout this paper $\|\cdot\|$ denotes the Euclidean vector norm. The coefficients α and β in (4) and (5) are positive regularization parameters similarly as in (3). We use the initial iterate

$$w^{(0)} := f^\delta \in \mathbb{R}^{n^2}. \quad (6)$$

The relation between $w^{(i)}$ and $w^{(i-1)}$, determined by (4) and (5), can be expressed as

$$w^{(i)} = T(w^{(i-1)}), \quad (7)$$

where

$$T(\cdot) = S_{tv}(S_h(\cdot)). \quad (8)$$

The following subsections discuss image deblurring with the operator S_h and denoising with the operator S_{tv} . Convergence properties when $\|\cdot\|_{tv}$ is the standard discrete TV-norm are investigated in Section 3.

2.1 Image deblurring

We consider the numerical solution of a sequence of discrete image deblurring problems (4) by an extension of the method proposed in [12], which is designed for the solution of (4) with a linear regularization operator. The solution method is based on partial Golub-Kahan bidiagonalization of the blurring matrix H . Application of ℓ steps of Golub-Kahan bidiagonalization to H with initial vector (6) yields the matrices $U_{\ell+1} \in \mathbb{R}^{n^2 \times (\ell+1)}$ and $V_\ell \in \mathbb{R}^{n^2 \times \ell}$ with orthonormal columns, and a lower bidiagonal matrix $\bar{C}_\ell \in \mathbb{R}^{(\ell+1) \times \ell}$ with positive subdiagonal entries such that

$$HV_\ell = U_{\ell+1}\bar{C}_\ell, \quad H^*U_\ell = V_\ell C_\ell^*, \quad U_{\ell+1}e_1 = f^\delta / \|f^\delta\|, \quad (9)$$

where $U_\ell \in \mathbb{R}^{n^2 \times \ell}$ is made up of the ℓ first columns of $U_{\ell+1}$, $C_\ell \in \mathbb{R}^{\ell \times \ell}$ consists of the first ℓ rows of \bar{C}_ℓ , the superscript $*$ denotes transposition, and $e_1 = [1, 0, \dots, 0]^*$ is the first axis vector. The columns of V_ℓ span the Krylov subspace

$$\mathcal{K}_\ell := \mathcal{K}_\ell(H^*H, H^*f^\delta) := \text{span}\{H^*f^\delta, (H^*H)H^*f^\delta, \dots, (H^*H)^{\ell-1}H^*f^\delta\};$$

see, e.g., Björck [3] for details on the decompositions (9). We assume ℓ to be small enough, so that these decompositions with the stated properties exist.

Let $L^{(i-1)} \in \mathbb{R}^{n^2 \times n^2}$ be a linearization of the discrete nonlinear operator L , cf. (4), and introduce its QR factorization

$$L^{(i-1)}V_\ell = Q_\ell R_\ell, \quad (10)$$

where $Q_\ell \in \mathbb{R}^{n^2 \times \ell}$ has orthonormal columns and $R_\ell \in \mathbb{R}^{\ell \times \ell}$ is upper triangular. Since $L^{(i-1)}$ is nonsingular, so is R_ℓ . Typically, R_ℓ is not very ill-conditioned.

Substituting $u = V_\ell y$ into (4) and using (10) yields the reduced minimization

problem

$$\begin{aligned} & \min_{y \in \mathbb{R}^\ell} \left\{ \|\bar{C}_\ell y - e_1 \|f^\delta\|^2 + \alpha \|R_\ell y - Q_\ell^* L^{(i-1)} w^{(i-1)}\|^2 \right\} \\ & = \min_{y \in \mathbb{R}^\ell} \left\| \begin{bmatrix} \bar{C}_\ell \\ \sqrt{\alpha} R_\ell \end{bmatrix} y - \begin{bmatrix} e_1 \|f^\delta\| \\ \sqrt{\alpha} Q_\ell^* L^{(i-1)} w^{(i-1)} \end{bmatrix} \right\|^2, \end{aligned} \quad (11)$$

where, for $i > 1$, $w^{(i-1)}$ is given by the previous alternating step, (5), and $w^{(0)}$ is given by (6). Since R_ℓ is nonsingular, the minimization problem (11) has a unique solution $y_\ell = y_{\ell, \alpha}$ for any $\alpha > 0$. The corresponding solution of (4) is given by

$$u^{(i)} = V_\ell y_\ell. \quad (12)$$

Let δ be an available bound for the Euclidean norm of the error in f^δ and let η be a user-specified constant. A vector u is said to satisfy the discrepancy principle if $\|Hu - f^\delta\| \leq \eta\delta$. We choose the regularization parameter α as large as possible so that the computed approximate solution (12) of (4) satisfies the discrepancy principle, i.e., so that

$$\|Hu_\ell - f^\delta\| = \eta\delta. \quad (13)$$

It follows from (9) and (12) that

$$\|Hu_\ell - f^\delta\| = \|\bar{C}_\ell y_\ell - e_1 \|f^\delta\|\|. \quad (14)$$

The determination of α such that (13) holds typically requires the solution of a sequence of fairly small least-squares problems (11), each one corresponding to a different value of α . We may solve these problems, e.g., by using the generalized singular value decomposition of the matrix pair $\{\bar{C}_\ell, R_\ell\}$. The following approach is an alternative, which avoids the fairly expensive computation of this decomposition. Moreover, it yields formulas that are helpful for our analysis. Let $\tilde{C}_\ell := \bar{C}_\ell R_\ell^{-1}$ and substitute $z := R_\ell y - Q_\ell^* L^{(i-1)} w^{(i-1)}$ into (11). This gives the equivalent minimization problem

$$\min_{z \in \mathbb{R}^\ell} \left\| \begin{bmatrix} \tilde{C}_\ell \\ \sqrt{\alpha} I \end{bmatrix} z - \begin{bmatrix} e_1 \|f^\delta\| - \tilde{C}_\ell Q_\ell^* L^{(i-1)} w^{(i-1)} \\ 0 \end{bmatrix} \right\|^2, \quad (15)$$

which can be solved efficiently as described in [9]. Denote the solution by $z_\ell = z_{\ell, \alpha}$. The associated solution of (11) is given by

$$y_\ell = R_\ell^{-1}(z_\ell + Q_\ell^* L^{(i-1)} w^{(i-1)}). \quad (16)$$

We are interested in how the function

$$\phi_\ell(\alpha) = \|\bar{C}_\ell y_\ell - e_1\| f^\delta \|^2 \quad (17)$$

depends on α .

Proposition 2.1 *The function (17) is continuous for $\alpha \geq 0$, strictly increasing for $\alpha > 0$, and satisfies*

$$\phi_\ell(0) = \|P_{\mathcal{N}(\bar{C}_\ell^*)} e_1\|^2 \|f^\delta\|^2, \quad (18)$$

$$\lim_{\alpha \rightarrow \infty} \phi_\ell(\alpha) = \|e_1\| f^\delta \|^2 - \|\tilde{C}_\ell Q_\ell^* L^{(i-1)} w^{(i-1)}\|^2, \quad (19)$$

where $P_{\mathcal{N}(\bar{C}_\ell^*)}$ denotes the orthogonal projector onto $\mathcal{N}(\bar{C}_\ell^*)$.

Proof. Related results for the situation when $w^{(i-1)}$ vanishes are shown in [12]. Recall that the matrix \bar{C}_ℓ is of full rank. The solution y_ℓ of (11) therefore is a continuous function of $\alpha \geq 0$ and so is ϕ_ℓ . Let $\alpha > 0$. The matrix identity

$$\tilde{C}_\ell(\tilde{C}_\ell^* \tilde{C}_\ell + \alpha I)^{-1} \tilde{C}_\ell^* - I = -(\alpha^{-1} \tilde{C}_\ell \tilde{C}_\ell^* + I)^{-1}$$

can be shown, e.g., with the aid of the singular value decomposition of \tilde{C}_ℓ . Using (16), the representation

$$z_\ell = (\tilde{C}_\ell^* \tilde{C}_\ell + \alpha I)^{-1} \tilde{C}_\ell^* (e_1\|f^\delta\| - \tilde{C}_\ell Q_\ell^* L^{(i-1)} w^{(i-1)})$$

of the solution of (15), and the above matrix identity, in order, yield

$$\begin{aligned} \bar{C}_\ell y_\ell - e_1\|f^\delta\| &= \tilde{C}_\ell z_\ell + \tilde{C}_\ell Q_\ell^* L^{(i-1)} w^{(i-1)} - e_1\|f^\delta\| \\ &= (\tilde{C}_\ell(\tilde{C}_\ell^* \tilde{C}_\ell + \alpha I)^{-1} \tilde{C}_\ell^* - I) e_1\|f^\delta\| \\ &\quad - (\tilde{C}_\ell(\tilde{C}_\ell^* \tilde{C}_\ell + \alpha I)^{-1} \tilde{C}_\ell^* - I) \tilde{C}_\ell Q_\ell^* L^{(i-1)} w^{(i-1)} \\ &= -(\alpha^{-1} \tilde{C}_\ell \tilde{C}_\ell^* + I)^{-1} (e_1\|f^\delta\| - \tilde{C}_\ell Q_\ell^* L^{(i-1)} w^{(i-1)}). \end{aligned}$$

Thus,

$$\phi_\ell(\alpha) = g^* (\alpha^{-1} \tilde{C}_\ell \tilde{C}_\ell^* + I)^{-2} g, \quad g := e_1\|f^\delta\| - \tilde{C}_\ell Q_\ell^* L^{(i-1)} w^{(i-1)}.$$

This representation shows that ϕ_ℓ is increasing for $\alpha > 0$, as well as the limit (19).

When $\alpha = 0$, the solution of (11) can be expressed as $y_\ell = (\bar{C}_\ell^* \bar{C}_\ell)^{-1} \bar{C}_\ell^* e_1\|f^\delta\|$. Substitution into (17) shows (18). \square

In view of (13) and (14), we would like the regularization parameter α to satisfy

$$\phi_\ell(\alpha) = \eta^2 \delta^2. \quad (20)$$

By Proposition 2.1, this equation has a unique solution, which we denote by α_{discr} , when $\eta^2\delta^2$ is bounded above by (19) and below by (18). A variety of methods can be applied to compute α_{discr} ; see, e.g., [4] for a discussion on a root-finder.

For very small values of ℓ , equation (20) might not have a solution because the lower bound (18) is larger than $\eta^2\delta^2$. In this situation, we increase the number of bidiagonalization steps ℓ . The following result provides a justification.

Proposition 2.2 *Assume that $P_{\mathcal{N}(\bar{C}_\ell^*)}e_1 \neq 0$. Then*

$$\|P_{\mathcal{N}(\bar{C}_{\ell+1}^*)}e_1\| < \|P_{\mathcal{N}(\bar{C}_\ell^*)}e_1\|.$$

Proof. The result follows from the fact that the matrices \bar{C}_j have positive subdiagonal entries. A proof for the situation when \bar{C}_j is an upper Hessenberg matrix with positive subdiagonal entries is provided in [25, Section 6.5.3] and is applicable to the present situation. We outline the proof, because this allows us to define quantities of later use.

It follows from (18), (17), and (11) that

$$\|P_{\mathcal{N}(\bar{C}_\ell^*)}e_1\|f^\delta\| = \min_{y \in \mathbb{R}^\ell} \|\bar{C}_\ell y - e_1\|f^\delta\|. \quad (21)$$

Introduce the QR factorization

$$\bar{C}_\ell = W_{\ell+1}\bar{R}_\ell, \quad (22)$$

where $W_{\ell+1} \in \mathbb{R}^{(\ell+1) \times (\ell+1)}$ has orthonormal columns and $\bar{R}_\ell \in \mathbb{R}^{(\ell+1) \times \ell}$ has a leading $\ell \times \ell$ upper triangular matrix. The matrix $W_{\ell+1}^*$ can be represented by a product of ℓ Givens rotations,

$$W_{\ell+1}^* = G_\ell G_{\ell-1} \cdots G_1,$$

where

$$G_j = \begin{bmatrix} I_{j-1} & & & \\ & c_j & s_j & \\ & -s_j & c_j & \\ & & & I_{\ell-j} \end{bmatrix} \in \mathbb{R}^{(\ell+1) \times (\ell+1)}.$$

The entries s_j and c_j are the sines and cosines of certain angles, determined so that \bar{R}_ℓ is upper triangular. In particular, the fact that \bar{C}_ℓ has nonvanishing subdiagonal entries guarantees that $0 < s_j < 1$ for all j . Substituting the QR

factorization (22) into the right-hand side of (21) yields

$$\min_{y \in \mathbb{R}^\ell} \|\bar{C}_\ell y - e_1\| \|f^\delta\| = \min_{y \in \mathbb{R}^\ell} \|W_{\ell+1} \bar{R}_\ell y - e_1\| \|f^\delta\| = |e_{\ell+1}^* W_{\ell+1}^* e_1| \|f^\delta\|.$$

The special form of $W_{\ell+1}^*$ shows that

$$|e_{\ell+1}^* W_{\ell+1}^* e_1| = |s_\ell| |e_\ell^* W_\ell^* e_1|,$$

from which the proposition follows. \square

By the proof of the above proposition, we have

$$\|P_{\mathcal{N}(\tilde{C}_\ell^*)} e_1\| \|f^\delta\| = |e_{\ell+1}^* W_{\ell+1}^* e_1| \|f^\delta\|.$$

The right-hand side easily can be evaluated for increasing values of ℓ and be used to determine the smallest value of ℓ for which

$$\|P_{\mathcal{N}(\tilde{C}_\ell^*)} e_1\| \|f^\delta\| < \eta \delta.$$

We denote this value by ℓ_{\min} . Thus, it is necessary that $\ell \geq \ell_{\min}$ in order for (20) to have a bounded solution.

We have observed in numerous numerical examples that letting ℓ be somewhat larger than ℓ_{\min} improves the quality of the computed restoration. For many restoration problems

$$\ell = \ell_{\min} + 15 \tag{23}$$

is a suitable choice in the sense that it gives better restorations than $\ell = \ell_{\min}$, and increasing ℓ further does not improve the quality of the restoration significantly.

The computational effort to determine the decompositions (9) when n^2 is large is dominated by the ℓ matrix-vector product evaluations required with each one of the matrices H and H^* . The matrix $L^{(i-1)}$ is very sparse; see below. Therefore, the computational effort needed to evaluate $L^{(i-1)} V_\ell$ typically is smaller than the work required for the evaluation of ℓ matrix-vector products with H .

2.2 Image denoising

The total variation method is a well-known approach to noise-removal. In the continuous setting, the method determines a denoised image w from a

noise-contaminated image u by solving

$$\min_w \left\{ \int_{\Omega} \frac{\alpha}{\beta} (\mathcal{L}(w - u))^2 + |\nabla w| dx \right\}, \quad (24)$$

usually with \mathcal{L} being the identity. In the discrete setting, we solve the analogous problem

$$w := \operatorname{argmin}_w \left\{ \frac{\alpha}{\beta} \|L^{(i-1)}(w - u)\|^2 + \|w\|_{tv} \right\}; \quad (25)$$

cf. (5). A variety of numerical methods for denoising by the TV-norm are available, including Chambolle's projection algorithm [5], the semi-smooth Newton method [19], multilevel optimization [6], and explicit or semi-implicit time-marching schemes [1,15,16].

Recently, Chen et al. [7] proposed an adaptive TV method, which replaces (24) by

$$\min_w \left\{ \int_{\Omega} \frac{\alpha}{\beta} \frac{\lambda(D)}{2} (\mathcal{L}(u - w))^2 + |\nabla w|^{p(D)} dx \right\}, \quad (26)$$

where the difference curvature

$$D := ||u_{\eta\eta}| - |u_{\xi\xi}||$$

is used as edge indicator. Here the second derivatives $u_{\eta\eta}$ and $u_{\xi\xi}$ are in the direction of the gradient and in a direction orthogonal to the gradient, respectively. The functions p and λ are defined by

$$p(D) := 2 - \sqrt{\bar{D}}, \quad \lambda(D) := \gamma \sqrt{\bar{D}}$$

with $\gamma > 0$ a regularization parameter and $\bar{D} := D/D_{\max}$ a normalization of D . Here D_{\max} denotes the maximal value of D over the whole image. Since $\bar{D} \in [0, 1]$, the function $p(D)$ decreases monotonically from 2 to 1 as \bar{D} increases, and $\lambda(D) \in [0, \gamma]$. At sharp edges, $p(D)$ is close to unity and $\lambda(D)$ is close to γ ; in smooth regions, $p(D)$ is about 2 and $\lambda(D)$ is close to zero.

The Euler-Lagrange equation associated with the minimization problem (26), supplied with a gradient descent that gives a minimizer of (26) as $t \rightarrow \infty$, is for $(x, t) \in \Omega \times [0, \infty)$ given by

$$\frac{\partial w}{\partial t} = \operatorname{div}(g(|\nabla w|)\nabla w) + \lambda(D)\mathcal{L}^*\mathcal{L}(u - w), \quad w = w(x, t), \quad (27)$$

with diffusivity

$$g(s) := p(D)s^{p(D)-2}; \quad (28)$$

see [7] for the case $\mathcal{L} = I$. Alternatively, the function g may be defined by

$$g(s) := 1/(1 + s^2/\rho^2) \quad (29)$$

with $\rho > 0$ a small positive constant, see [23] for discussions on this choice of diffusivity, or by

$$g(s) := 1/s \quad (30)$$

as in classical Total Variation models. We determine a (partially) denoised image by integrating a discrete version of (27) a few “time-steps.”

We conclude this subsection with a discussion on the linearization and discretization of the regularization operator

$$\mathcal{L}(w) = \operatorname{div}(g(|\nabla w|)\nabla w). \quad (31)$$

Here ∇w denotes the gradient of w considered as a real-valued function defined in \mathbb{R}^2 . We first linearize (31) by evaluating g at $|\nabla w|$ using w from the previous time-step, i.e.,

$$\mathcal{L}(w^{(i)}) \approx \operatorname{div}(g(|\nabla w^{(i-1)}|)\nabla w^{(i)}). \quad (32)$$

Discretization of (32) gives the matrix $L^{(i)} \in \mathbb{R}^{n^2 \times n^2}$ with, generically, five nonvanishing entries in each row. The entries in the row associated with pixel (k, j) are determined by the values of the image w at pixel (k, j) and at the four adjacent pixels in the horizontal and vertical directions, denoted by N , S , E , and W . Thus, the row of $L^{(i)}$ associated with pixel (k, j) is, generically, of the form

$$\{l_{k,j,S}, 0, \dots, 0, l_{k,j,E}, -(l_{k,j,S} + l_{k,j,E} + l_{k,j,W} + l_{k,j,N}), l_{k,j,W}, 0, \dots, 0, l_{k,j,N}\}$$

with elements

$$l_{k,j,E} := \frac{1}{2}(g_{k,j} + g_{k+1,j}), \quad l_{k,j,W} := \frac{1}{2}(g_{k,j} + g_{k-1,j}),$$

$$l_{k,j,S} := \frac{1}{2}(g_{k,j} + g_{k,j-1}), \quad l_{k,j,N} := \frac{1}{2}(g_{k,j} + g_{k,j+1}),$$

where $g_{k,j}$ represents an approximation of the diffusivity $g(|\nabla w|)$ at pixel (k, j) . Partial derivatives are approximated by central finite differences,

$$g_{k,j} := g\left(\left(\frac{w_{k+1,j} - w_{k-1,j}}{2}\right)^2 + \left(\frac{w_{k,j+1} - w_{k,j-1}}{2}\right)^2\right),$$

where $w_{k,j}$ denotes the value of w at pixel (k, j) . Expressions for $l_{k,j,S}$ and $l_{k,j,N}$ can be derived similarly; see [26] for details. Other discretizations are discussed in [10].

The matrix $L^{(0)}$ is in initial computations determined by integrating

$$\frac{\partial w}{\partial t} = \operatorname{div}(g(|\nabla w|)\nabla w)$$

a few time-steps (5 in the computed examples) with a suitably chosen function g . Then $L^{(0)}$ is used in the first step of the alternating method. Iteration i of the alternating method uses the regularization matrix $L^{(i-1)}$ for deblurring (4) and denoising (5). After the i th iteration, we update the regularization matrix $L^{(i-1)}$ to obtain the new regularization matrix $L^{(i)}$, exploiting available derivative information.

3 Convergence analysis

We show convergence of the alternating method (4)-(5) by adapting the proof by Huang et al. [13] to the method of the present paper. Following Huang et al. [13], we would like to show that the operator T in (8) is nonexpansive and asymptotically regular. We assume in this section that the regularization operator \mathcal{L} is linear; hence the matrix $L = L^{(i)}$ is independent of i . This assumption can be weakened and replaced by suitable conditions on the family of matrices $\{L^{(i)}\}_{i=0}^{\infty}$.

Introduce the vector or induced matrix norms

$$\|\cdot\|_L := \|L \cdot\|. \tag{33}$$

An operator $W : \mathbb{R}^{n^2} \rightarrow \mathbb{R}^{n^2}$ is said to be nonexpansive (with respect to the norm (33)) if

$$\|W(x) - W(y)\|_L \leq \|x - y\|_L \quad \forall x, y \in \mathbb{R}^{n^2},$$

and W is said to be asymptotically regular if for any $x \in \mathbb{R}^{n^2}$,

$$\lim_{j \rightarrow \infty} \|W^{j+1}(x) - W^j(x)\|_L = 0.$$

The following result will be used to show that the iterates $w^{(i)}$, $i = 1, 2, 3, \dots$, determined by (7) converge.

Theorem 3.1 [22, Theorem 1] *Let C be a closed convex set in a Hilbert space X and let $W : C \rightarrow C$ be a nonexpansive asymptotically regular mapping for which the set F of fixed points is nonempty. Then, for any $x \in C$, the sequence of successive approximations $\{T^j x\}$ is weakly convergent to an element of F .*

Let the function φ be convex, lower semicontinuous, and not identically $+\infty$, and let α be a positive constant. Then the functional

$$S(y) := \operatorname{argmin}_{x \in \mathbb{R}^{n^2}} \{\|y - x\|_L^2 + \alpha\varphi(x)\}$$

is nonexpansive; see [8, Lemma 2.4]. It follows that the operator S_{tv} defined by (5) is nonexpansive.

Lemma 3.1 *The operator T defined by (8) is nonexpansive for all $\alpha > 0$.*

Proof. Since the operator S_{tv} is nonexpansive, it follows that

$$\|T(x) - T(y)\|_L = \|S_{tv}(S_h(x)) - S_{tv}(S_h(y))\|_L \leq \|S_h(x) - S_h(y)\|_L,$$

and (4) yields

$$\|S_h(x) - S_h(y)\|_L = \|(H^*H + \alpha L^*L)^{-1}\alpha L^*L(x - y)\|_L.$$

The identity

$$L(H^*H + \alpha L^*L)^{-1}\alpha L^*L = \left(\frac{1}{\alpha} L^{-*}H^*HL^{-1} + I\right)^{-1}L$$

for $\alpha > 0$ shows that

$$\|(H^*H + \alpha I)^{-1}\alpha L^*Lx\|_L = \left\|\left(\frac{1}{\alpha} L^{-*}H^*HL^{-1} + I\right)^{-1}Lx\right\| \leq \|x\|_L,$$

where the inequality follows from the fact that

$$\left\|\left(\frac{1}{\alpha} L^{-*}H^*HL^{-1} + I\right)^{-1}\right\| \leq 1 \quad \forall \alpha > 0.$$

This shows the lemma. \square

It is convenient to introduce the discrete analogue of the functional in (3),

$$J(u, w) := \|Hu - f^\delta\|^2 + \alpha\|L(u - w)\|^2 + \beta\|w\|_{tv}. \quad (34)$$

The following result is used to show that the operator T is asymptotically regular.

Lemma 3.2 *The sum*

$$\sum_{i=1}^{\infty} \|w^{(i-1)} - w^{(i)}\|_L^2 \quad (35)$$

is convergent for the sequence $w^{(0)}, w^{(1)}, w^{(2)}, \dots$ defined by (7).

Proof. Let the functional J be defined by (34). Expanding $u \rightarrow J(u, w^{(i)})$ around $u = u^{(i+1)}$ and then letting $u = u^{(i)}$ yields

$$\begin{aligned} J(u^{(i)}, w^{(i)}) &= J(u^{(i+1)}, w^{(i)}) + (\nabla_u J(u^{(i+1)}, w^{(i)}))^*(u^{(i)} - u^{(i+1)}) \\ &\quad + \frac{1}{2}(u^{(i)} - u^{(i+1)})^* \nabla_u^2 J(u^{(i+1)}, w^{(i)})(u^{(i)} - u^{(i+1)}), \end{aligned}$$

where ∇_u and ∇_u^2 denote the gradient and Hessian of J with respect to u , respectively. Since $u^{(i+1)}$ is the minimizer of $J(u, w^{(i)})$, we have $\nabla_u J(u^{(i+1)}, w^{(i)}) = 0$. Moreover, $\nabla_u^2 J(u^{(i+1)}, w^{(i)}) = 2(H^*H + \alpha L^*L)$. It follows that

$$\begin{aligned} J(u^{(i)}, w^{(i)}) - J(u^{(i+1)}, w^{(i)}) &= (u^{(i)} - u^{(i+1)})^*(H^*H + \alpha L^*L)(u^{(i)} - u^{(i+1)}) \\ &= (u^{(i)} - u^{(i+1)})^* L^*(L^{-*}H^*HL^{-1} + \alpha I)L(u^{(i)} - u^{(i+1)}) \\ &\geq \alpha \|u^{(i)} - u^{(i+1)}\|_L^2. \end{aligned}$$

In view of that $w = w^{(i+1)}$ is a minimizer of $w \rightarrow J(u^{(i)}, w)$, we have

$$J(u^{(i)}, w^{(i)}) - J(u^{(i+1)}, w^{(i+1)}) \geq J(u^{(i)}, w^{(i)}) - J(u^{(i+1)}, w^{(i)})$$

and, therefore,

$$J(u^{(i)}, w^{(i)}) - J(u^{(i+1)}, w^{(i+1)}) \geq \alpha \|u^{(i)} - u^{(i+1)}\|_L^2.$$

Finally, because the operator S_{tw} is nonexpansive, we obtain

$$\|u^{(i)} - u^{(i+1)}\|_L^2 \geq \|S_{tw}(u^{(i)}) - S_{tw}(u^{(i+1)})\|_L^2 = \|w^{(i)} - w^{(i+1)}\|_L^2.$$

It follows that the sum (35) with nonnegative terms is bounded and therefore converges. \square

Corollary 3.1 *The operator T defined by (8) is asymptotically regular.*

Proof. By the convergence of the sum (35), we have $\lim_{i \rightarrow \infty} \|w^{(i+1)} - w^{(i)}\|_L = 0$. The corollary now follows from the observation that $w^{(i+1)} - w^{(i)} = T^{i+1}w^{(0)} - T^i w^{(0)}$. \square

In view of Theorem 3.1, we have established convergence of the sequence (7) to a fixed point of T provided that a fixed point exists. To show existence, we introduce the notions of proper and coercive functions.

Let $\psi : \mathbb{R}^{n^2} \rightarrow \mathbb{R}$ and let $\mathcal{X} \subset \mathbb{R}^{n^2}$. The function ψ is said to be proper over \mathcal{X} if $\psi(x) < \infty$ for at least one point $x \in \mathcal{X}$ and $\psi(x) > -\infty$ for all $x \in \mathcal{X}$. We say that ψ is coercive over \mathcal{X} if for every sequence $x^{(0)}, x^{(1)}, x^{(2)}, \dots$ in \mathcal{X} with $\lim_{i \rightarrow \infty} x^{(i)} = \infty$, we have $\lim_{i \rightarrow \infty} \psi(x^{(i)}) = \infty$.

The existence of a fixed point of the mapping T is shown with the help of the following result; see, e.g., Bertsekas [2, Proposition 2.1.1] for a proof.

Lemma 3.3 *Let $\psi : \mathbb{R}^{n^2} \rightarrow \mathbb{R}$ be a closed, proper, and coercive function. Then the set of minima of ψ in \mathbb{R}^{n^2} is nonempty and compact.*

Lemma 3.4 *Let D_x and D_y be matrices of one-sided finite difference approximations of first order derivatives in the horizontal and vertical directions, respectively, and define the matrix*

$$D = \begin{bmatrix} D_x \\ D_y \end{bmatrix}.$$

The functional J defined by (34) is coercive in \mathbb{R}^{n^2} provided that the null spaces for H and D intersect trivially.

Proof. Since we assume the regularization matrix L to be nonsingular, the result follows similarly as Huang et al. [13, Lemma 2.7]. \square

The restriction of the matrix H to the null space of D typically is well conditioned for image restoration problems. We therefore may assume that the conditions of Lemma 3.4 hold. Combining the results of this section shows convergence of the alternating method to a minimizer of (34).

Theorem 3.2 *Assume that the conditions of Lemmas 3.3 and 3.4 hold, let L be nonsingular, and let the regularization parameter α be positive. Then the alternating method determines a sequence of elements $w^{(0)}, w^{(1)}, w^{(2)}, \dots$ in \mathbb{R}^{n^2} that converge to a minimum of the functional (34).*

We remark that if H is of full rank, then the functional (34) is strictly convex and has a unique minimum.

4 Numerical experiments

This section illustrates the performance of the alternating methods defined by (4)-(5). The methods differ in the choice of regularization operator. Given a representation of the blur- and noise-free image $\hat{u} \in \mathbb{R}^{n^2}$, we determine a blur- and noise-contaminated image $f^\delta \in \mathbb{R}^{n^2}$ from

$$f^\delta = H\hat{u} + e.$$

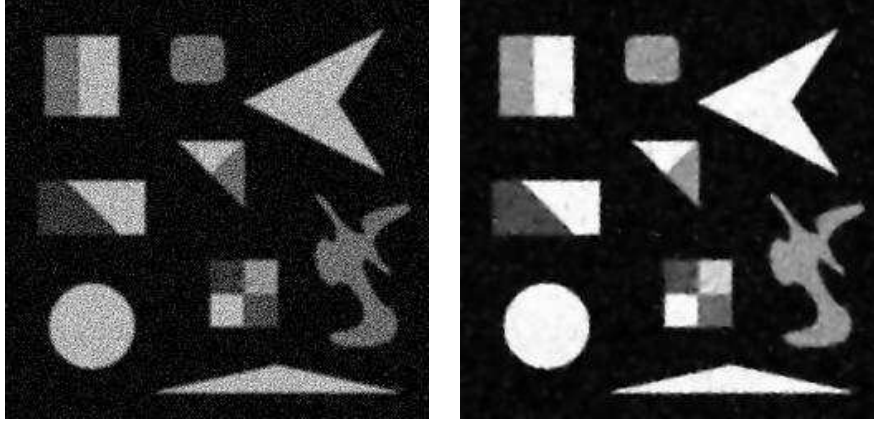


Fig. 1. Example 4.1: Restoration of corrupted version of the `corner` image: (left) the corrupted image produced by Gaussian blur, determined by the parameters `band = 5` and `sigma = 3`, and by 30% noise; (right) restored image determined by 3 steps of the alternating method.

The “noise vector” $e \in \mathbb{R}^{n^2}$ has normally distributed entries with mean zero, scaled to yield a desired noise-level

$$\nu = \frac{\|e\|}{\|\hat{u}\|}, \quad (36)$$

from which we determine the value of δ in (13). Our task is to compute an accurate approximation of \hat{u} given f^δ , H , and δ , by the alternating iterative method (4)-(5). We terminate the iterations and accept $w^{(i)}$ as the computed approximation of \hat{u} as soon as the relative difference between consecutive iterates $w^{(1)}, w^{(2)}, w^{(3)}, \dots$ is sufficiently small; specifically, we accept $w^{(i)}$ when for the first time

$$\|w^{(i)} - w^{(i-1)}\|/\|w^{(i)}\| < 1 \cdot 10^{-4}. \quad (37)$$

The displayed restored images provide a qualitative measure of the performance of the alternating methods. The signal-to-noise ratio

$$\text{SNR}(w^{(i)}, \hat{u}) = 20 \log_{10} \frac{\|\hat{u}\|}{\|w^{(i)} - \hat{u}\|} \text{ dB},$$

is a quantitative measure of the quality of $w^{(i)}$. A high SNR-value indicates that the restoration is accurate; however, we note that the SNR-value is not always in agreement with visual perception.

In the deblurring step (4) of the alternating method, we apply regularization operators of the kind described in Subsection 2.2, unless explicitly stated otherwise. In order to reduce the computational effort, we use the operator $L^{(i-1)} = I$ in the denoising step (5) in all computed examples. The latter is a

ν	SNR_i	SNR_{Sh}	SNR_{Stv}
0.15	14.94	17.59	18.26
0.30	10.95	15.06	16.30

Table 1

Example 4.1: Results for restorations of **corner** images that have been corrupted by Gaussian blur, determined by `band` = 3 and `sigma` = 3, and by noise corresponding to noise-level ν .

consequence of applying $\mathcal{L} = I$ in (27). The choice of the identity regularization operator in (5) is computationally more efficient than using a more general regularization operator, and the loss of quality of the restored images in terms of SNR-values generally is negligible. The latter is illustrated in Example 4.3.

The parameter α/β in (25) determines the penalty applied to the fidelity term. The regularization parameter α is obtained by solving (20) and we let $\beta := 40\alpha$.

Example 4.1. We consider the restoration of blur- and noise-contaminated **corner** images. They are represented by 256×256 pixels, i.e., $n = 256$.

The matrix H represents a Gaussian blurring operator and is generated with the MATLAB function `blur.m` from Regularization Tools [11]. This function has two parameters `band` and `sigma`. The former specifies the half-bandwidth of the Toeplitz blocks and the latter the variance of the Gaussian point spread function. The larger `sigma`, the more blurring. Enlarging `band` increases the storage requirement, the arithmetic work necessary for the evaluation of matrix-vector products with H , and to some extent the blurring. We use regularization operators $L^{(i-1)}$ of the kind described at the end of Subsection 2.2 in the deblurring step (4) of the alternating method.

Tables 1 and 2 show results obtained after the first iteration step with the alternating method. Table 1 reports SNR-values for the case when the available image **corner** is corrupted by much noise and modest Gaussian blur, characterized by `band` = 3 and `sigma` = 3. The parameter η in (13) is set to 0.9 in this example. We remark that in (non-alternating) iterative methods that solve equation (4) only, η should generally be chosen larger than unity; see, e.g., [12] for computed examples. However, we noticed experimentally that letting $\eta < 1.0$ is beneficial in our alternating method. The deblurring step (4) yields a worse but sharper image with $\eta < 1$ than when $\eta > 1$ is used. This image subsequently is improved by the denoising step (5). The number of bidiagonalization steps, $\ell = 17$, is determined by (23).

The first column of Table 1 shows the noise level (36) and the second column, labeled SNR_i , reports the SNR-values of the available contaminated image f^δ , i.e., $\text{SNR}(\hat{u}, f^\delta)$. The columns labeled SNR_{Sh} and SNR_{Stv} display SNR-values

band	sigma	ℓ	SNR _{<i>i</i>}	SNR _{<i>Sh</i>}	SNR _{<i>Stv</i>}
7	5	29	11.98	14.44	16.18
9	3	28	11.48	14.91	15.19

Table 2

Example 4.1: Results for restorations of **corner** images that have been corrupted by Gaussian blur corresponding to different **band** and **sigma** values, and by 5% noise. The parameter ℓ shows the number of bidiagonalization steps.

for the restored images obtained after the initial deblurring step (4) and after the subsequent denoising step (5), respectively. Denoising is seen to increase the SNR-value considerably.

Letting the alternating method proceed until the stopping criterion (37) is satisfied yields the restored image $w^{(3)}$ with SNR = 18.33 for $\nu = 0.15$, and SNR = 16.65 for $\nu = 0.30$. The contaminated blurred and noisy image represented by f^δ is shown on the left-hand side of Figure 1 and the restoration $w^{(3)}$ is depicted on the right-hand side of Figure 1.

For comparison, we applied the denoising step (5) with $L^{(i-1)} = I$, only, to the image **corner** corrupted by Gaussian blur and noise of level $\nu = 0.30$. The restored image obtained after 31 iterations has SNR = 14.04. This illustrates that the deblurring step is essential even when the available image f^δ is corrupted by modest blur, only.

Table 2 presents results obtained for **corner**-images that are contaminated by fairly little noise ($\nu = 0.05$) and significant Gaussian blur. The number of bidiagonalization steps is determined by (23) and is displayed in the table. The table shows SNR-values for restored images obtained after the first deblurring step (SNR_{*Sh*}) and after the subsequent denoising step (SNR_{*Stv*}). We observe that, as can be expected, the major improvement is due to the deblurring step.

If we continue the iterations until the stopping criterion (37) is satisfied, then we obtain $w^{(2)}$ with SNR = 16.48 for the first row of Table 2 and SNR = 15.28 for the second row of Table 2. \square

L	SNR _{<i>i</i>}	SNR _{<i>f</i>}
I	15.71	19.68
L_p	15.71	20.08
L_c	15.71	19.91
L_t	15.71	19.87

Table 3

Example 4.2: Results for restorations determined with different regularization operators L . The corrupted image is contaminated by Gaussian blur (**band** = 7, **sigma** = 1.5) and 10% noise.

L	SNR_i	SNR_f
I	5.00	15.71
L_p	5.00	16.10
L_c	5.00	16.07
L_t	5.00	15.92

Table 4

Example 4.2: Results for restorations determined with different regularization operators L . The corrupted image is contaminated by linear motion blur ($\text{width} = 15$, $\theta = 15$) and 10% noise.

L	SNR_i	SNR_f
I	10.74	15.15
L_p	10.74	15.28
L_c	10.74	15.26
L_t	10.74	15.18

Table 5

Example 4.2: Results for restorations determined with different regularization operators L . The corrupted image is contaminated by spatially variant Gaussian blur ($\text{band} = 15$, $\text{sigma}_1 = 9$, $\text{sigma}_2 = 3$) and 10% noise.

Example 4.2. We compare the alternating methods with different regularization operators applied to the restoration of 800×800 -pixel **zebra**-images that have been corrupted by spatially variant Gaussian blur, spatially invariant Gaussian blur, or motion blur, as well as by noise.

The PSF for linear motion blur is represented by a line segment of length r pixels in the direction of the motion. The angle θ (in degrees) specifies the direction and is measured counter-clockwise from the positive x -axis. The PSF takes on the value r^{-1} on this segment and vanishes elsewhere. We refer to the parameter r as the **width**. The larger the **width**, the more ill-conditioned the matrix H , and the more difficult the restoration task.

The contamination caused by spatially variant Gaussian blur is determined by the nonsymmetric blurring matrix given by

$$H := I_1(T_1 \otimes T_1) + I_2(T_2 \otimes T_2) \in \mathbb{R}^{n^2 \times n^2}. \quad (38)$$

Here I_1 is the diagonal matrix, whose first $n^2/2$ diagonal entries are one, and the remaining entries vanish, and $I_2 := I - I_1$. The operator \otimes denotes the Kronecker product and the T_ℓ are banded Toeplitz matrices, which represent Gaussian blur in one space-dimension. Specifically, $T_\ell = [t_{jk}^{(\ell)}]_{j,k=1}^n$ is defined

by

$$t_{jk}^{(\ell)} := \begin{cases} \frac{1}{\sigma_\ell \sqrt{2\pi}} \exp\left(-\frac{(j-k)^2}{2\sigma_\ell^2}\right), & \text{if } |j-k| \leq \mathbf{band}, \\ 0, & \text{otherwise.} \end{cases}$$

The blurring matrix (38) models the situation when the left and right halves of the image are degraded by different Gaussian blurs. The matrix H is non-symmetric; its first $n^2/2$ rows are made up of the first $n^2/2$ rows of $T_1 \otimes T_1$, and its last $n^2/2$ rows are the last $n^2/2$ rows of $T_2 \otimes T_2$.

Tables 3, 4, and 5 show restoration results achieved with alternating methods using different regularization operators when applied to **zebra** images that have been contaminated by symmetric Gaussian blur (**band** = 9, **sigma** = 9), motion blur (**width** = 15, θ = 15), and spatially variant Gaussian blur (**band** = 15, **sigma**₁ = 9, **sigma**₂ = 3), respectively, as well as by 10% noise. The SNR-values for the available contaminated images f^δ are displayed in the columns labeled SNR_{*i*}. The columns labeled SNR_{*f*} show SNR-values for restored images $w^{(i)}$ that satisfy the stopping criterion (37). For regularization in (4), we use the identity I , the matrix L_p determined by the diffusivity (29), the matrix L_c defined by the diffusivity (28), and the matrix L_t determined by (30). The regularization operator L_p is seen to yield restorations with the highest SNR-values.

The regularization matrices different from I are updated after each denoising step (5). If we, instead, keep $L = L_p$ fixed throughout the iterations with the alternating methods, restorations with somewhat smaller SNR-values result. We obtain SNR = 19.97 for the contaminated image of Table 3, SNR = 15.97 for the contaminated image of Table 4, and SNR = 15.22 for the contaminated image of Table 5.

Figure 2 displays the exact (uncorrupted), corrupted, and restored **zebra** images and a region of special interest, which is zoomed in and shown in the bottom row. The exact image is depicted in Figure 2(a). A version that has been contaminated by linear motion blur, determined by **width**= 15 and θ = 15, and by 10% noise is displayed in Figure 2(b), and the restored image determined by our alternating method with $L = L_p$ is shown in Figure 2(c).

We let $\eta = 0.95$ in (13) in all computations for this example. The number of bidiagonalization steps (23) is for all regularization operators about 18. \square

Example 4.3. The purpose of this example is to discuss the use of the regularization operator $L = I$ in (5). We consider the restoration of 800×800 -pixel **zebra**-images that have been contaminated by Gaussian blur for different values of the parameters **band** and **sigma**. The number of bidiagonalization steps is chosen according to (23) and we let $\eta = 0.95$ in (13).

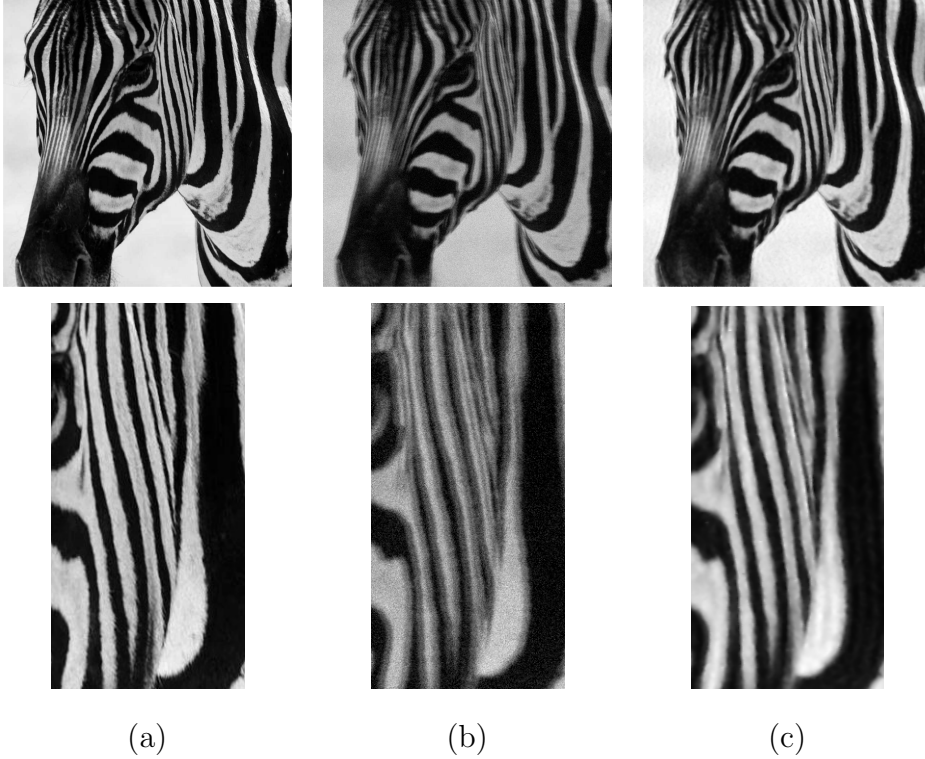


Fig. 2. Example 4.2: (a) Blur- and noise-free image, (b) image contaminated by linear motion blur and 10% noise, and (c) restoration determined by alternating method with regularization operator L_p . The bottom row shows a zoomed in region of special interest.

band, sigma	SNR _i	L	SNR _f	iter
21, 21	7.51	I	12.26	2
21, 21	7.51	L_p	12.29	2
11, 11	11.04	I	15.96	3
11, 11	11.04	L_p	15.97	3
9, 9	12.17	I	17.00	2
9, 9	12.17	L_p	17.04	2
5, 5	15.28	I	19.42	2
5, 5	15.28	L_p	19.44	2

Table 6

Example 4.3: SNR-values for restorations of zebra-images corrupted by different Gaussian blurs, determined by the parameters **band** and **sigma**, and by 10% noise. The performance of the regularization parameters $L = I$ and $L = L_p$ in (5) is compared.

Table 6 reports SNR-values obtained when using $L = I$ and $L = L_p$ in the denoising step (5) of the alternating method. In the deblurring step, we apply

$L = L_p$. The first column of the table displays the values of the parameters `band` and `sigma` used to define the Gaussian blurring matrix H . The column labeled SNR_i displays the SNR-values for the blur- and noise-contaminated images to be restored, i.e., the values $\text{SNR}(f^\delta, \hat{u})$. The column labeled L shows the regularization operator used in the denoising step (5), and the column labeled SNR_f reports SNR-values for the restored images. The last column shows the number of iterations required by the alternating method to satisfy the stopping criterion (37). Table 6 shows that the gain in SNR-values for the restored images is very small, at most 0.25%, when using the regularization operator L_p instead of the identity as regularization operator in (5). We therefore use $L = I$ in (5) in all computed examples, because this choice reduces the computational work. \square

<code>band, sigma</code>	ν	SNR_i	SNR_f	SNR_m
5, 3	0.15	12.72	15.99	18.75
5, 3	0.10	13.14	16.81	19.02
5, 3	0.05	14.15	17.79	23.49
7, 5	0.15	10.51	14.40	14.63
7, 5	0.10	11.61	15.02	18.43
7, 5	0.05	11.98	16.24	21.24

Table 7

Example 4.4: SNR-values for corrupted and restored `corner`-images. Contamination is by Gaussian blur defined by the parameters `band` and `sigma`, and by noise of level ν .

<code>band, sigma</code>	ν	SNR_i	SNR_f	SNR_m
5, 3	0.15	7.29	11.10	7.63
5, 3	0.10	8.54	12.15	10.83
5, 3	0.05	9.50	13.00	12.44
7, 5	0.15	5.98	9.64	7.63
7, 5	0.10	6.83	10.22	9.58
7, 5	0.05	7.48	11.34	10.71

Table 8

Example 4.4: SNR-values for corrupted and restored `butterfly`-images. Contamination is by Gaussian blur defined by the parameters `band` and `sigma`, and by noise of level ν .

Example 4.4. We compare the alternating method with $L = L_p$ defined by (29) with a nonconvex nonsmooth minimization method, which uses total variation (TV) regularization, proposed by Nikolova et al. [20]. This state-of-the-art method is related to our model when $\mathcal{L} = I$. We use software made available by the authors [21].

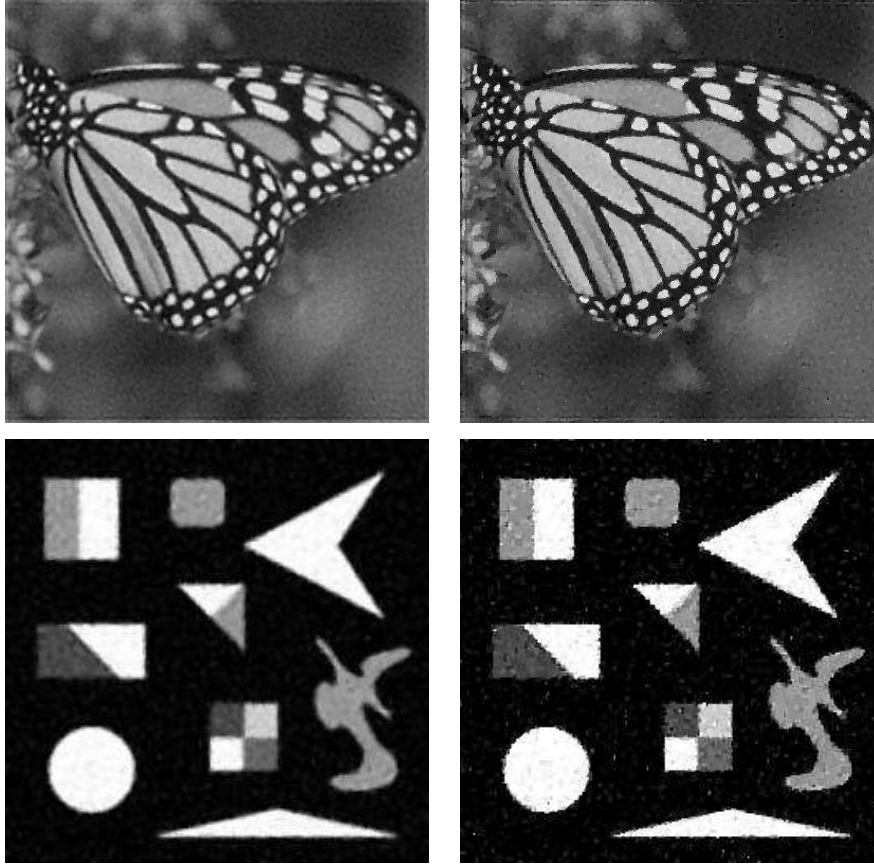


Fig. 3. Example 4.4: Left column: images restored by our alternating method; right column: images restored by the minimization method [20].

The contaminated images are corrupted by Gaussian blur defined by the parameters `band` and `sigma` and by noise of level ν ; cf. (36). Tables 7 and 8 report SNR-values for the available contaminated images in the columns labeled SNR_i , SNR-values for the restored images determined by our alternating method in the columns labeled SNR_f , and SNR-values for the restored images determined by the minimization method [20] in the columns labeled SNR_m . Table 7 is for the `corner` image and Table 8 for a 400×400 -pixel `butterfly` image.

The tables and many additional numerical experiments indicate that the relative performance of the methods compared strongly depends on the kind of image. The approach in [20] performs better for blocky images, while for photographic images our alternating method gives more accurate restorations, because our approach restores fine details better. This is illustrated in Figure 3.

We remark that the software [21] failed when applied to images with much noise ($> 15\%$). We therefore do not report these results in tables. This may depend on some design or parameter choices in [21]. \square

5 Conclusion

This paper describes a new alternating method for image deblurring and denoising. Deblurring is carried out by a Krylov subspace iterative method based on partial Golub-Kahan bidiagonalization of the blurring matrix, while denoising is performed by the adaptive TV method proposed in [7]. Our approach allows the application of regularization operators that are constructed from the differential operator used in the denoising step. This makes the computation of the regularization operator inexpensive.

Acknowledgments

We would like to thank a referee for comments. This work is supported by MIUR-Prin Grant 20083KLJEZ and by ex 60% project by the University of Bologna “Funds for selected research topics.”

References

- [1] D. Bertaccini and F. Sgallari, Updating preconditioners for nonlinear deblurring and denoising image restoration, *Applied Numer. Math.*, 60 (2010), pp. 994–1006.
- [2] D. Bertsekas, *Convex Analysis and Optimization*, Athena Scientific, Belmont, MA, 2003.
- [3] Å. Björck, *Numerical Methods for Least Squares Problems*, SIAM, Philadelphia, 1996.
- [4] D. Calvetti and L. Reichel, Tikhonov regularization of large linear problems, *BIT*, 43 (2003), pp. 263–283.
- [5] A. Chambolle, An algorithm for total variation minimization and applications, *J. Math. Imaging Vis.*, 20 (2004), pp. 89–97.
- [6] T. F. Chan and K. Chen, An optimization-based multilevel algorithm for total variation image denoising, *Multiscale Model. Simul.*, 5 (2006), pp. 615–645.
- [7] Q. Chen, P. Montesinos, Q. S. Sun, P. A. Heng, and D. S. Xia, Adaptive total variation denoising based on difference curvature, *Image and Vision Computing*, 28 (2010), pp. 298–306.
- [8] P. L. Combettes and V. R. Wajs, Signal recovery by proximal forward-backward splitting, *Multiscale Model. Simul.*, 4 (2005), pp. 1168–1200.

- [9] L. Eldén, Algorithms for the regularization of ill-conditioned least squares problems, *BIT*, 17 (1977), pp. 134–145.
- [10] A. Handlovičová, K. Mikula, and F. Sgallari, Semi-implicit complementary volume scheme for solving level set like equations in image processing and curve evolution, *Numer. Math.*, 93 (2003), pp. 675–695.
- [11] P. C. Hansen, Regularization tools version 4.0 for Matlab 7.3, *Numer. Algorithms*, 46 (2007), pp. 189–194.
- [12] M. E. Hochstenbach and L. Reichel, An iterative method for Tikhonov regularization with a general linear regularization operator, *J. Integral Equations Appl.*, 22 (2010), pp. 463–480.
- [13] Y. Huang, M. K. Ng, and Y.-W. Wen, A fast total variation minimization method for image restoration, *Multiscale Model. Simul.*, 7 (2008), pp. 774–795.
- [14] F. Li, M. K. Ng, and R. J. Plemmons, Coupled segmentation and denoising/deblurring models for hyperspectral material identification, preprint, 2009. Available at <http://www.wfu.edu/~plemmons/papers.html>
- [15] A. Marquina and S. Osher, Explicit algorithms for a new time dependent model based on level set motion for nonlinear deblurring and noise removal, *SIAM J. Sci. Comput*, 22 (2000), pp. 387–405.
- [16] S. Morigi, L. Reichel, F. Sgallari, and A. Shyshkov, Cascadic multiresolution methods for image deblurring, *SIAM J. Imaging Sci.*, 1 (2008), pp. 51–74.
- [17] S. Morigi, L. Reichel, and F. Sgallari, Noise-reducing cascadic multilevel methods for linear discrete ill-posed problems, *Numer. Algorithms*, 53 (2010), pp. 1–22.
- [18] S. Morigi, L. Reichel, and F. Sgallari, Cascadic multilevel methods for fast nonsymmetric blur- and noise-removal, *Appl. Numer. Math.*, 60 (2010), pp. 378–396.
- [19] M. Ng, L. Qi, Y. Yang, and Y. Huang, On semismooth Newton’s methods for total variation minimization, *J. Math. Imaging Vis.*, 27 (2007), pp. 265–276.
- [20] M. Nikolova, M. Ng, and C. Tam, Fast nonconvex nonsmooth minimization methods for image restoration and reconstruction, *IEEE Trans. Image Processing*, to appear.
- [21] M. Nikolova, M. Ng, and C. Tam, Software is available at <http://www.math.hkbu.edu.hk/~mng/imaging-software.html>
- [22] Z. Opial, Weak convergence of the sequence of successive approximations for nonexpansive mappings, *Bull. Amer. Math. Soc.*, 73 (1967), pp. 591–597.
- [23] P. Perona and J. Malik, Scale-space and edge detection using anisotropic diffusion, *IEEE Trans. Pattern Analysis and Machine Intelligence*, 12 (1990), pp. 629–639.

- [24] L. Reichel, F. Sgallari, and Q. Ye, Tikhonov regularization based on generalized Krylov subspace methods, *Appl. Numer. Math.*, in press.
- [25] Y. Saad, *Iterative Methods for Sparse Linear Systems*, 2nd ed., SIAM, Philadelphia, 2003.
- [26] J. Weickert, B. M. H. Romeny, and M. A. Viergever, Efficient and reliable schemes for nonlinear diffusion filtering, *IEEE Trans. Image Processing*, 7 (1998), pp. 398–410.
- [27] Y.-W. Wen, M. K. Ng, and W.-K. Ching, Iterative algorithms based on decoupling of deblurring and denoising for image restoration, *SIAM J. Sci. Comput.*, 30 (2008), pp. 2655–2674.